

Unusual evolution of B_{c2} and T_c with inclined fields in restacked TaS₂ nanosheets

Yonghui Ma^{1,3,4}, Jie Pan^{2,4}, Chenguang Guo^{2,4}, Xuan Zhang¹, Lingling Wang¹, Tao Hu^{1,3}, Gang Mu^{1,3,*}, Fuqiang Huang^{2,3,†}, and Xiaoming Xie^{1,3,4}

Recently we reported an enhanced superconductivity in restacked monolayer TaS₂ nanosheets compared with the bulk TaS₂, pointing to the exotic physical properties of low dimensional systems. Here we tune the superconducting properties of this system with magnetic field along different directions, where a strong Pauli paramagnetic spin-splitting effect is found in this system. Importantly, an unusual enhancement as high as 3.8 times of the upper critical field B_{c2} , as compared with the Ginzburg-Landau (GL) model and Tinkham model, is observed under the inclined external magnetic field. Moreover, with the out-of-plane field fixed, we find that the superconducting transition temperature T_c can be enhanced by increasing the in-plane field and forms a dome-shaped phase diagram. An extended GL model considering the special microstructure with wrinkles was proposed to describe the results. The restacked crystal structure without inversion center along with the strong spin-orbit coupling may also play an important role for our observations.

¹State Key Laboratory of Functional Materials for Informatics, Shanghai Institute of Microsystem and Information Technology, Chinese Academy of Sciences, Shanghai 200050, China. ²State Key Laboratory of High Performance Ceramics and Superfine Microstructure, Shanghai Institute of Ceramics, Chinese Academy of Sciences, Shanghai, 200050, China. ³Center for Excellence in Superconducting Electronics (CENSE), Chinese Academy of Sciences, Shanghai 200050, China. ⁴University of Chinese Academy of Sciences, Beijing 100049, China. Correspondence and requests for materials should be addressed to G.M. (email: mugang@mail.sim.ac.cn) and F.Q.H. (email: huangfq@mail.sic.ac.cn). Y.H.M. and J.P. contributed equally to this work.

Introduction

Superconductivity in low-dimensional systems was investigated extensively recently, due to the fertile physical phenomenon and exotic properties¹⁻⁴. At present, the gate of this research field has just been opened and more interesting phenomena are waiting to be explored. Because of the strong spin-orbit coupling, superconducting transition metal dichalcogenides (TMDs) are investigated intensively in the two-dimensional (2D) limit in recent years⁵⁻⁸. A clear enhancement of the in-plane upper critical field was frequently reported in these materials, which was interpreted by the Zeeman-protected Ising superconductivity mechanism. Using a chemical exfoliation method, we have obtained the monolayer TaS₂ nanosheets, which were assembled layer-by-layer by vacuum filtration^{9,10}. Such a restacked material shows superconductivity with T_c (~ 3.2 K) several times higher than the pristine bulk 2H-TaS₂, which supplies a significant platform for studying the intrinsic physical properties of unconventional superconductivity in TMDs. Such an enhancement of T_c is consistent with a previous work by E. N. Moratalla et al¹¹, although they didn't reach the one-layer limit, and finally confirmed by other two groups by mechanically exfoliating TaS₂ to monolayer^{12,13}. The enhancement of T_c was believed to originate from the suppression of the charge-density wave and the increase of the density of states by the process of thickness reduction.^{9,12} However, an in-depth investigation on the physical behaviors of the restacked TaS₂ is lacking and more experiments are required at present. Magnetic field is one of the fundamental tuning parameters to affect the behaviors of a superconductor. In the type-II superconductors, the magnetic field can penetrate into the bulk in the form of quantized vortex lines when it exceeds the lower critical field B_{c1} ¹⁴. In addition, various pair-breaking effect, including the orbital and

Zeeman type, can be induced by the magnetic field.

Here we present a detailed investigation on the Abrikosov vortex phase of the above-mentioned superconductor, restacked TaS₂ nanosheets, by measuring the conducting properties with magnetic fields along different directions. The in-plane upper critical field B_{c2}^{ab} is clear larger than the Pauli paramagnetic limiting fields B_P , indicating a strong Pauli paramagnetic spin-splitting effects in this material. Importantly, the angle dependence of the upper critical field deviates severely from the Ginzburg-Landau (GL) model and Tinkham model. Moreover, the value of T_c is found to increase with the in-plane field $B_{\parallel ab}$ under a fixed out-of-plane field $B_{\parallel c}$. Both the intrinsic and extrinsic origins for the observations were discussed and we found that the highly noncentrosymmetric crystal structure, the strong spin-orbit coupling, and the special microstructure with wrinkles are important factors for the unusual behaviors we observed.

Results

Details regarding the samples preparation and resistance measurements are given in the Methods section. By a careful characterization using combining methods, the structure of the restacked TaS₂ was determined and reported in our previous paper ⁹. The inter-layer spacing is close to bulk 2H-TaS₂, while the 2H symmetry has been broken after the restacking process because of rotations between different layers (see Fig. S1). In such a structure, both the in-plane inversion symmetry in each individual layer and the global inversion symmetry are broken. As a consequent, the inversion symmetry breaking will be severer than the bulk, monolayer, and few layered TaS₂

materials. The morphology of the samples were checked by the scanning electron microscope (SEM) and scanning transmission electron microscope (STEM) measurements. Wrinkles can be seen on the flat surface and oxides exist only at the edge of the sample with the width of several nanometers. The content of lithium ions was found to be below the minimum detection limit by the inductively coupled plasma optical emission spectrometer (ICP-OES) measurement. A clear Meissner effect can be seen from the magnetic susceptibility measurements (see Fig. S3d). These characterizations can be found in the Supplementary information.

The resistive transitions of one sample (denoted as #1) measured in magnetic fields for both orientations $B \parallel ab$ and $B \parallel c$ are shown in Figs. 1a and b. Clear different efficiencies for the suppression of superconductivity, revealing the anisotropy of the present material, can be seen by comparing the two figures. To determine the upper critical fields B_{c2} , a criterion of 90% of the normal state resistivity (ρ_n) is used and the results are shown in the Fig. 1c for the two orientations. Instead of the square root behavior for the in-plane upper critical field ($B_{c2}^{ab} \sim \sqrt{1 - T/T_c}$) expected for the 2D superconductors^{5-8,12}, an opposite tendency with a positive curvature is observed. This has been found to be a universal feature of anisotropic three-dimensional (3D) layered superconductors^{15,16}. This reflects the influence of inter-layer coupling on the in-plane upper critical field of our samples, although such an inter-layer stacking manner doesn't affect T_c . The value of B_{c2} at zero temperature can be estimated using the Werthamer-Helfand-Hohenberg relation¹⁷ $B_{c2} = -0.693 \times dB_{c2}(T)/dT|_{T_c} \times T_c$ after the slope $dB_{c2}(T)/dT|_{T_c}$ is obtained from Fig. 1c. In addition, the paramagnetic limiting field B_P has a simple relation with T_c , $B_P = 1.84 \times T_c$ based on the conventional BCS theory¹⁸. The resultant values for the three characteristic fields B_{c2}^{ab} (in-

plane B_{c2}), B_{c2}^c (out-of-plane B_{c2}) and B_P are denoted by arrows in Figure 1c and summarized in Table 1, from which the anisotropy of upper critical field $\Gamma = B_{c2}^{ab}/B_{c2}^c = 11$ is obtained. This value is larger than most of the iron-based superconductors and the copper-based superconductor YBCO^{16,19}. Moreover, a clear relative relation $B_{c2}^c < B_P < B_{c2}^{ab}$ can be deduced.

Field-angle resolved experiments were performed by measuring the field (B) and angle (θ) dependence of resistivity at a fixed temperature 2.2 K. As shown in Fig. 2a, one can see how the resistivity is triggered by the field from zero to finite values and saturates gradually at high fields. In order to determine the precise onset superconducting transition point, which reflects the information of upper critical fields B_{c2} , we show the first derivative $d\rho/dB$ of four typical curves in Fig. 2b. As indicated by the arrows, the onset transition point is defined by the characteristic field where the value of $d\rho/dB$ begins to increase clearly. The characteristic points determined in Fig. 2b are represented by arrows in Fig. 2a, the connection of which forms a slightly inclined straight line as shown by the blue dashed line. Based on this line reflecting the normal states resistance ρ_n , a criterion of $90\%\rho_n$, as revealed by the black dashed line, is adopted to define the upper critical fields. The crossing points between this black dashed line and the data curves in Fig. 2a determine the upper critical field at different angles $B_{c2}(\theta)$. Angle dependence of $B_{c2}(\theta)$ normalized by B_{c2}^c is shown in Fig. 2c. One can see the detailed evolution of $B_{c2}(\theta)/B_{c2}^c$ versus θ . In order to quantitatively evaluate such an angle dependent variation, we employ two theoretical models, the 3D GL model and 2D Tinkham model^{20,21} (see SI), and plot the curves based on them for comparison. These two models show slight differences near $\theta = 0^\circ$, which is usually used to distinguish the 2D superconductivity in monolayer or interfacial systems^{6,7,22}. However,

the difference between our experimental data and the two models is much larger, showing a great enhancement of upper critical field in a wide angle range. In the strong anisotropic system, the perpendicular component of the the upper critical field $B_{c2}(\theta)\sin\theta$ is expected to be dominant in the low angle range since the in-plane magnetic field is not important in terms of suppressing T_c . So we show this component normalized by B_{c2}^c in Fig. 2d, where a broad peak-shaped experimental curve with the maximum enhancement of 3.8 times is observed.

Actually such an upper-critical-field-enhancement effect can induce very fascinating features in T_c in the mixed state. Here we adopt a different mode of measurements: $\rho - T$ curves are measured with the out-of-plane field $B_{\parallel c}$ fixed and the in-plane field $B_{\parallel ab}$ increasing, as schematized in the inset of Fig. 3b. The current is applied in the direction perpendicular to $B_{\parallel ab}$. This method has been used to identify the 2D or interfacial superconductivity, where the curves will overlap with each other because $B_{\parallel ab}$ is not important in an extremely 2D superconductor^{22,23}. While in an anisotropic system with 3D features, T_c will be reasonably suppressed by $B_{\parallel ab}$ (see section 7 of SI). In Fig. 3a we show a typical set of data with $B_{\parallel c} = 0.4$ T on another sample denoted as #2 with a similar T_c as #1. The behavior is uniquely different from the above-mentioned two categories. The superconducting transition is enhanced clearly following by a suppression with the increasing of $B_{\parallel ab}$. Three criterions, 10% ρ_n , 50% ρ_n , and 90% ρ_n , are employed to determine the critical transition temperature T_c and the results are shown in Fig. 3b. All the three curves show the dome-like features, confirming that it is an intrinsic property rather than a magnetic flux-related behavior. The dome-like behavior may reveal the presence of competing between some unconventional effect and the pairing-breaking effect induced by magnetic field. Figure 3c summarizes

the effect of $B_{\parallel ab}$ on T_c at different $B_{\parallel c}$, where T_c is determined using the criterion $50\%\rho_n$. The maximum T_c for the three curves emerges at the same ratio $B_{\parallel ab}/B_{\parallel c}$, indicating a characteristic angle $\theta \sim 20^\circ$, along which the detrimental effect of magnetic field is mostly suppressed.

Discussion

The detailed investigations on the thickness dependence of superconducting behaviors of 2H-TaS₂¹² supply a good coordinate to make a comparison with our results. It is found that the critical transition temperature T_c increases with the decrease of thickness and reaches 3.4 K for monolayer TaS₂. This value is very close to our sample, confirming the monolayer-features of our sample and suggesting that the restacking process imposed on the monolayer TaS₂ doesn't affect T_c of this system. Moreover, the normal state resistivity displays a $T^{2.45}$ behavior in low temperature in our sample (see Fig. S4), corresponding to the situation between 3-layer ($\sim T^2$) and 7-layer ($\sim T^3$) for the ordered stacked TaS₂¹². This implies that the inter-layer coupling in our samples shows a certain degree of influence on the electrical transport behavior. A more careful examination shows that the out-of-plane upper critical field B_{c2}^c is similar to the bilayer TaS₂, while the in-plane B_{c2}^{ab} and the anisotropy are only one third of the bilayer TaS₂. Nevertheless, B_{c2}^{ab} of our samples is clearly larger than that of the bulk samples since the latter doesn't exceed the Pauli limit. All in all, the present samples are different from both the monolayered and the bulk TaS₂. The restacked TaS₂ monolayers maintain the enhanced T_c (compared with the bulk material), while lose the 2D characters and show an anisotropic 3D features. This is the basis of the following discussions.

Field-induced superconductivity has been theoretically proposed for ferromagnetic materials and is known as Jaccarino-Peter compensation effect.²⁴ In this effect, the internal magnetic field created by the magnetic moments through the exchange interaction can be compensated by the external magnetic field and superconductivity will occur. This mechanism has been realized in Eu-Sn molybdenum chalcogenides experimentally.²⁵ Moreover, another theory proposed by Kharitonov and Feigelman considered the polarization of magnetic impurity spins induced by the in-plane field and predicted an enhancement of superconductivity, especially in disordered films.²⁶ Evaluating the performances of our samples, we found that neither of the two theories is applicable. First of all, our magnetization measurement shows a paramagnetic behavior in our samples (see Fig. S3(c)), which excludes the presence of long-range magnetic moments and magnetic impurities. Secondly, the enhancement of T_c by in-plane field in our samples can only be observed in the presence of out-of-plane field, which is rather different from the case of the above-mentioned scenarios.

Intuitively, the theoretical proposal²⁷⁻²⁹ predicting a field-induced triplet component in the order parameter of the singlet superconductors due to the Pauli paramagnetic spin-splitting effect is very consistent with our observation shown in Fig. 2(d). According to their arguments, such an enhancement of $B_{c2}(\theta)$ should be conspicuous in anisotropic superconductors with $B_{c2}^c \ll B_P \ll B_{c2}^{ab}$. However, we note that such an exotic behavior is absent in so many low-dimensional TMDs with even stronger Pauli paramagnetic spin-splitting effect^{6,7}, which weakens the persuasion of this interpretation. Other important factors should be considered to interpret our experiments. One important clue for exploring the physical origination is that such a rare behavior was also

observed in restacked 1T'-MoS₂ (see Fig. S7) prepared with the similar process³⁰ to that used in restacked TaS₂. This implies that the unique and common features of such restacked monolayered materials are key factors for our observations. One most conspicuous feature for such restacked monolayer materials is the noncentrosymmetric crystal structure as mentioned in the beginning of the Results section. It has been discussed a lot both theoretically and experimentally that the noncentrosymmetric crystal structure along with strong spin-orbit coupling (SOC), which also exists in the present compound with 5d metal, is very favorable to incur the spin-triplet component in the superconducting order parameter^{31–37}. This may be one possible origin of our observations. One positive evidence for this scenario is that the restacked 1T'-MoS₂, which have a weaker SOC because of the lighter 4d Mo element, shows an inconspicuous enhancement of $B_{c2}(\theta)$ compared with restacked TaS₂ (see Fig. S7).

One possible extrinsic origination to explain our results comes from the possible orientation mismatch or wrinkles (see Fig. S2) of the monolayer TaS₂ sheets during the restacking process, which affects the c -axis orientation of the restacked samples. In section 9 of SI, we carefully analyzed the influences of different orientations on the estimation of B_{c2} and found that B_{c2} is mainly determined by the high- T_c portion where the included angle between the surface and field is the smallest. The presence of the low- T_c portion with a larger included angle can lower the onset transition temperature slightly (see Fig. S8). The simple GL model²⁰ is not applicable any more in this case. Considering the misaligned angle $\Delta\theta$ resulting from the wrinkles as schematically displayed in the inset of Fig. 4, we proposed an extended GL (EGL) model:

$$B_{c2}(\theta) = [1 - A(\theta)] \times \frac{B_{c2}^c}{\sqrt{\cos^2\Theta/\gamma^2 + \sin^2\Theta}}, \quad (1)$$

where $\Theta = \min |\theta - \Delta\theta|$ is the smallest included angle between the surface and field, and $A(\theta)$ is an adjusting parameter taking into account the effect of the low- T_c portion with other orientations. Here we simply assume that $A(\theta)$ is proportional to the GL formula, because $A(\theta)$ will be larger when T_c is more sensitive with the orientation, which can be reflected by the GL formula. Typically the misaligned angle $\Delta\theta$ has a distribution range with a maximum $\Delta\theta_{Max}$. Then we have

$$\Theta = \begin{cases} \theta - \Delta\theta_{Max}, & \theta > \Delta\theta_{Max} \\ 0. & \theta \leq \Delta\theta_{Max} \end{cases} \quad (2)$$

By tuning the value of parameters, it is found that when $\Delta\theta_{Max} = 27^\circ$, this EGL model can well describe the experimental data in the range $\theta > \Delta\theta_{Max}$, as shown in Fig. 4a. As for the case of $\theta \leq \Delta\theta_{Max}$, $B_{c2}(\theta)$ is only determined by the adjusting parameter $A(\theta)$. However, the influence factors on $A(\theta)$ are rather complicated in this region, so we could not get a good description at present. At this stage, we could not exclude the possibility that the wrinkles have an important influence on our observations. Even in this scenario, our results supplied an interesting prototypical system showing an unambiguous relationship between the microstructure and the physical (superconducting) performance. Moreover, this is also valuable in designing devices for applications.

It is notable that the enhancement of T_c by $B_{\parallel ab}$ at the present of $B_{\parallel c}$ is simply a natural consequence of the unusual behavior in $B_{c2}(\theta)$. As shown in Fig. 4b and 4c, supposing a linear

suppression of B_{c2} with the temperature approaching T_c : $B_{c2}(T) \sim 1 - T/T_c$, angle dependence of $B_{c2}(\theta)$ at other temperatures can be derived from the data at 2.2 K for both the experimental data and GL model, respectively. The total values of field in the experiment of Fig. 3, $\sqrt{B_{\parallel ab}^2 + B_{\parallel c}^2}$, are also plotted for comparison. The intersections between the two sets of curves indicate the values of T_c . With the decrease of θ , the intersection in Fig. 4b moves to high temperatures until the orientation around $20 - 30^\circ$, and then moves to low temperatures for both cases with $B_{\parallel c} = 0.2$ T and $B_{\parallel c} = 0.4$ T. This reproduces the variation of T_c with angle as shown in Figs. 3b and 3c. In the normal situation as shown in Fig. 4c, the value of $\sqrt{B_{\parallel ab}^2 + B_{\parallel c}^2}$ evolves along the tracing of GL model of a certain temperature in a rather wide angle range and moves to low temperature slightly in low angle region.

To summarize, we have measured angle-resolved electrical resistivity of the restacked TaS₂ nanosheets under magnetic field along different directions. It is found that Pauli paramagnetic limit is broken through in the mixed state, placing the present superconducting system in the environment suffering a strong Pauli paramagnetic spin-splitting effect. A clear enhancement of the upper critical field, as compared with the GL model and Tinkham model, is observed in inclined magnetic field. The critical transition temperature can be enhanced by the in-plane field at the presence of the out-of-plane field. Our analysis indicates that the highly noncentrosymmetric crystal structure, the strong spin-orbit coupling and the special microstructure with wrinkles are important factors for the mechanism of the unusual behaviors we observed.

Methods

Sample preparation. The restacked TaS₂ nanosheets were obtained by a chemical exfoliation method followed by the vacuum filtration^{9,10}. Firstly 2H-TaS₂ powders were prepared by the solid-state reaction. Then the Li_xTaS₂ powders were synthesized by soaking as-prepared 2H-TaS₂ powders in n-butyl lithium solution. The as-prepared Li_xTaS₂ crystals were exfoliated in distilled water. The redox reaction occurs at this stage. The obtained colloidal solution is composed of TaS₂ monolayers and is rather stable. The restacked TaS₂ nanosheets were obtained from the vacuum filtration of the colloidal suspension. The restacked TaS₂ samples are stable in air within 24 hours (see Fig. S2).

Morphology characterization. The morphology of restacked TaS₂ nanosheets was characterized by JSM-6510 scanning electron microscope (SEM). The atomic structures were observed through JEOL ARM-200F High-angle annular dark field (HAADF) scanning transmission electron microscope (STEM).

Resistance measurements. The restacked samples for the electrical transport measurements have the thickness of about 1 μm . The electrical transport data were collected by the standard four-probe method with magnetic field rotating in the plane perpendicular to the electric current. θ denoted the included angle between external field B and the ab -plane of the crystal. The applied electric current is 10 μA when carrying out the resistivity measurements and up to 50 mA for the I-V measurements.

Data availability. All relevant data are available from the corresponding author.

Acknowledgments

This work is supported by the Youth Innovation Promotion Association of the Chinese Academy of Sciences (No. 2015187), the National Natural Science Foundation of China (No. 11204338), and the “Strategic Priority Research Program (B)” of the Chinese Academy of Sciences (No. XDB04040300).

Author contributions

G.M. and F.Q.H. designed the experiments. Y.H.M. performed the measurements. J.P. and C.G.G. synthesized the samples. G.M. analysed the data. Y.H.M., J.P., C.G.G. X.Z., L.L.W., T.H., G.M., F.Q.H., and X.M.X. discussed the results. G.M. and F.Q.H. wrote the paper. X.M.X. supervised the work.

Additional information

Supplementary information accompanies the paper on the npj Quantum Materials website.

Competing Interests: The authors declare no competing financial and non-financial interests.

References

1. Reyren, N. *et al.* Superconducting interfaces between insulating oxides. *Science* **317**, 1196–1199 (2007).

2. Gozar, A. *et al.* High-temperature interface superconductivity between metallic and insulating copper oxides. *Nature* **455**, 782–785 (2008).
3. Wang, Q.-Y. *et al.* Interface-induced high-temperature superconductivity in single unit-cell fese films on SrTiO₃. *Chin. Phys. Lett.* **29**, 037402 (2012).
4. Saito, Y., Nojima, T. & Iwasa, Y. Highly crystalline 2D superconductors. *Nat. Rev. Mat.* **2**, 16094 (2016).
5. Xi, X. *et al.* Ising pairing in superconducting NbSe₂ atomic layers. *Nat. Phys.* **12**, 139–143 (2016).
6. Saito, Y. *et al.* Superconductivity protected by spin-valley locking in ion-gated MoS₂. *Nat. Phys.* **12**, 144–149 (2016).
7. Lu, J. M. *et al.* Evidence for two-dimensional ising superconductivity in gated MoS₂. *Science* **350**, 1353–1357 (2015).
8. Xing, Y. *et al.* Ising superconductivity and quantum phase transition in macro-size monolayer NbSe₂. *Nano Lett.* **17**, 6802–6807 (2017).
9. Pan, J. *et al.* Enhanced superconductivity in restacked TaS₂ nanosheets. *J. Am. Chem. Soc.* **139**, 4623–4626 (2017).
10. Guo, C. *et al.* High-quality single-layer nanosheets of MS₂ (M = Mo, Nb, Ta, Ti) directly exfoliated from AMS₂ (A = Li, Na, K) crystals. *J. Mater. Chem. C* **5**, 5977–5983 (2017).

11. Moratalla, E. N. *et al.* Enhanced superconductivity in atomically thin TaS₂. *Nat. Commun.* **7**, 11043 (2016).
12. Yang, Y. *et al.* Enhanced superconductivity and suppression of charge-density wave order in 2H-TaS₂ in the two-dimensional limit. *arXiv*: 1711.00079 (2017).
13. de la Barrera, S. C. *et al.* Tuning ising superconductivity with layer and spin-orbit coupling in two-dimensional transition-metal dichalcogenides. *Nat. Commun.* **9**, 1427 (2018).
14. Abrikosov, A. A. *Fundamentals of Theory of Metals* (Elsevier, 1988).
15. Woollam, J. A. & Somoano, R. B. Superconducting critical fields of alkali and alkaline-earth intercalates of MoS₂. *Phys. Rev. B* **13**, 3843–3853 (1976).
16. Ma, Y. *et al.* Strong anisotropy effect in an iron-based superconductor CaFe_{0.882}Co_{0.118}AsF. *Supercond. Sci. Technol.* **30**, 074003 (2017).
17. Werthamer, N. R., Helfand, E. & Hohenberg, P. C. Temperature and purity dependence of the superconducting critical field, H_{c2} . III. electron spin and spin-orbit effects. *Phys. Rev.* **147**, 295–302 (1966).
18. Clogston, A. M. Upper limit for the critical field in hard superconductors. *Phys. Rev. Lett.* **9**, 266–267 (1962).
19. Yuan, F. F. *et al.* Anisotropy of iron-platinum-arsenide Ca₁₀(Pt_{*n*}As₈)(Fe_{2–*x*}Pt_{*x*}As₂)₅ single crystals. *Appl. Phys. Lett.* **107**, 012602 (2015).

20. Blatter, G., Feigel'man, M. V., Geshkenbein, V. B., Larkin, A. I. & Vinokur, V. M. Vortices in high-temperature superconductors. *Rev. Mod. Phys.* **66**, 1125–1388 (1994).
21. Harper, F. E. & Tinkham, M. The mixed state in superconducting thin films. *Phys. Rev.* **172**, 441–450 (1968).
22. Zhou, W. *et al.* Anomalous electron doping independent two-dimensional superconductivity. *New J. Phys.* **19**, 073014 (2017).
23. Wu, J. *et al.* Anomalous independence of interface superconductivity from carrier density. *Nat. Mater.* **12**, 877–881 (2013).
24. Jaccarino, V. & Peter, M. Ultra-high-field superconductivity. *Phys. Rev. Lett.* **9**, 290–292 (1962).
25. Meul, H. W. *et al.* Observation of magnetic-field-induced superconductivity. *Phys. Rev. Lett.* **53**, 497–500 (1984).
26. Kharitonov, M. Y. & Feigelman, M. V. Enhancement of superconductivity in disordered films by parallel magnetic field. *JETP Lett.* **82**, 421–425 (2005).
27. Lebed, A. G. Cooper pairs with broken parity and spin-rotational symmetries in *d*-wave superconductors. *Phys. Rev. Lett.* **96**, 037002 (2006).
28. Lebed, A. G. Type-IV superconductivity: Can superconductivity be more exotic than unconventional? *J. Low Temp. Phys.* **142**, 173–178 (2006).

29. Dutta, O. & Lebed, A. G. Cooper pairs with broken time-reversal, parity, and spin-rotational symmetries in singlet type-II superconductors. *Phys. Rev. B* **78**, 224504 (2008).
30. Guo, C. *et al.* Observation of superconductivity in 1T'-MoS₂ nanosheets. *J. Mater. Chem. C* **5**, 10855–10860 (2017).
31. Gor'kov, L. P. & Rashba, E. I. Superconducting 2D system with lifted spin degeneracy: Mixed singlet-triplet state. *Phys. Rev. Lett.* **87**, 037004 (2001).
32. Frigeri, P. A., Agterberg, D. F., Koga, A. & Sigrist, M. Superconductivity without inversion symmetry: MnSi versus CePt₃Si. *Phys. Rev. Lett.* **92**, 097001 (2004).
33. Samokhin, K. V. Paramagnetic properties of noncentrosymmetric superconductors: Application to CePt₃Si. *Phys. Rev. Lett.* **94**, 027004 (2005).
34. Frigeri, P. A., Agterberg, D. F. & Sigrist, M. Spin susceptibility in superconductors without inversion symmetry. *New J. Phys.* **6**, 115 (2004).
35. Yuan, H. Q. *et al.* S-wave spin-triplet order in superconductors without inversion symmetry: Li₂Pd₃B and Li₂Pt₃B. *Phys. Rev. Lett.* **97**, 017006 (2006).
36. Nishiyama, M., Inada, Y. & Zheng, G.-q. Spin triplet superconducting state due to broken inversion symmetry in Li₂Pt₃B. *Phys. Rev. Lett.* **98**, 047002 (2007).
37. Yogi, M. *et al.* Evidence for novel pairing state in noncentrosymmetric superconductor CePt₃Si: ²⁹Si-NMR knight shift study. *J. Phys. Soc. Jpn.* **75**, 013709 (2006).

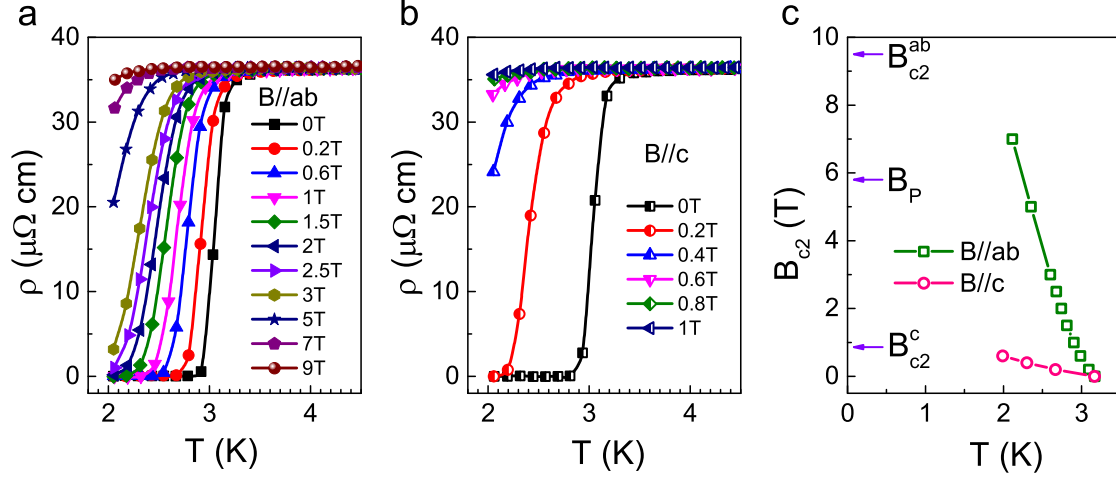


Figure 1: Temperature dependence of the resistive transitions under magnetic field for the sample #1. (a) $B \parallel ab$. (b) $B \parallel c$. (c) $B_{c2} - T$ phase diagram obtained using the criterion $90\%R_n$. The three characteristic fields B_{c2}^{ab} , B_{c2}^c and B_P are indicated by the arrows in this figure.

Figure captions

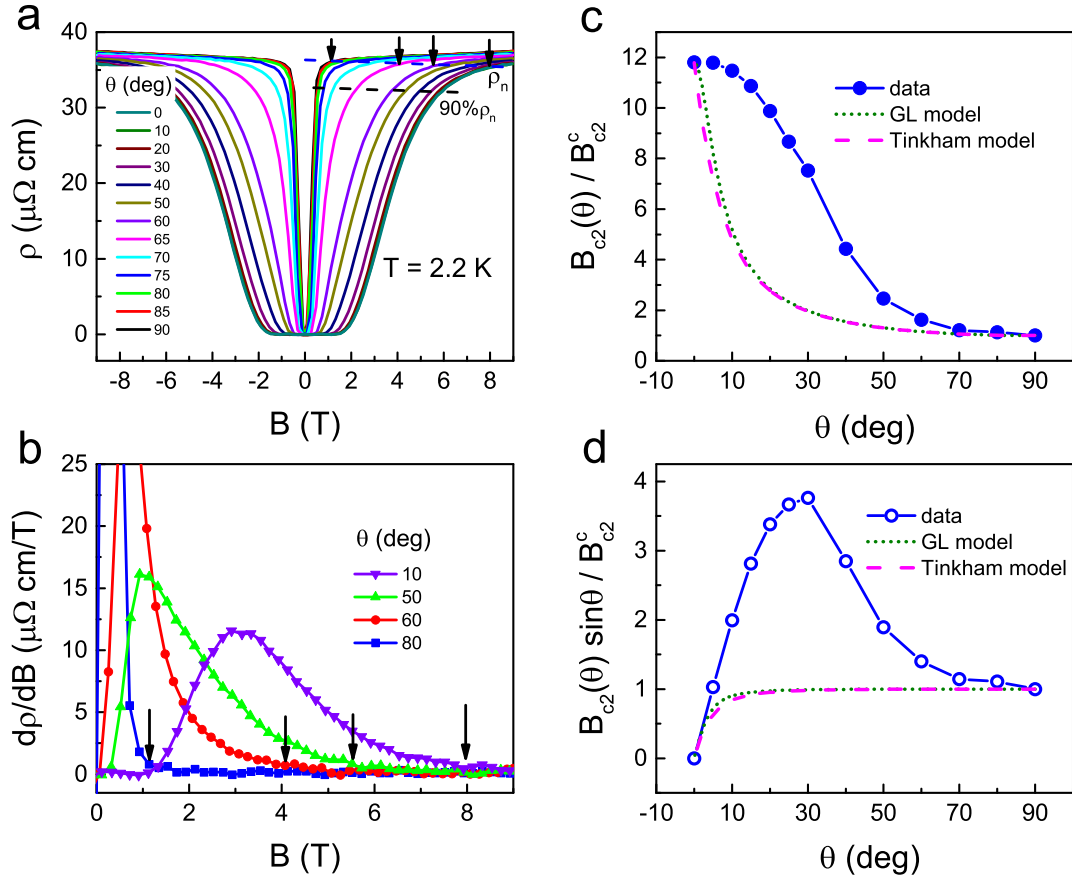


Figure 2: The measurements of the upper critical field along different directions $B_{c2}(\theta)$ for sample #1. (a) Field dependence of resistivity with the external field rotating from $B \parallel ab$ ($\theta = 0^\circ$) to $B \parallel c$ ($\theta = 90^\circ$) at a fixed temperature $T = 2.2 \text{ K}$. (b) Differential of the $\rho - B$ curves in (a), based on which the onset superconducting transition points are determined indicated by the black arrows. (c) Angular dependence of the upper critical field $B_{c2}(\theta)$ normalized by B_{c2}^c . (d) Field dependence of perpendicular component of the upper critical field $B_{c2}(\theta) \sin \theta$ normalized by B_{c2}^c . In (c) and (d), the theoretical curves based on the GL model and Tinkham model are shown in comparison with the experimental data.

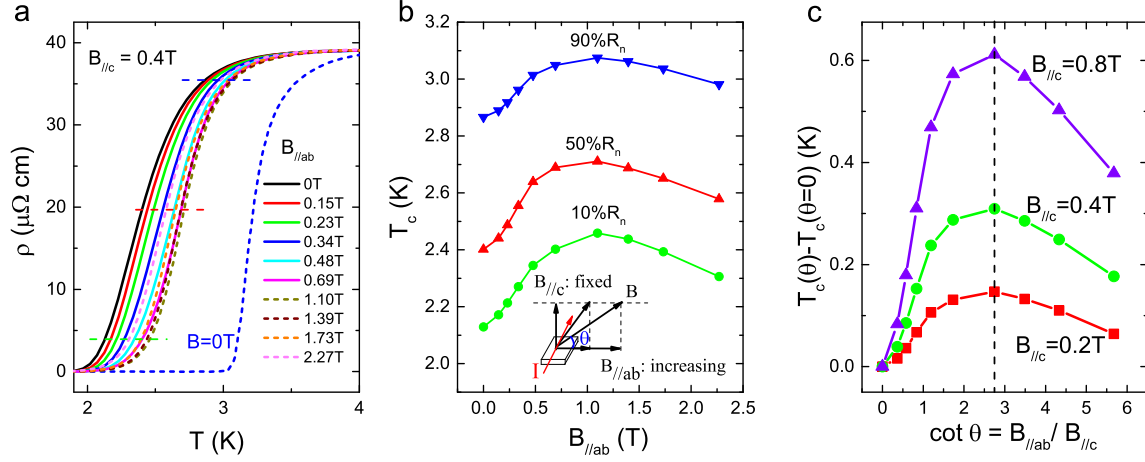


Figure 3: Electrical resistivity data and the critical transition temperature in the inclined field with $B_{||c}$ fixed and $B_{||ab}$ increasing for sample #2. (a) $\rho - T$ curves with $B_{||c} = 0.4 \text{ T}$ and $B_{||ab}$ increasing. (b) $B_{||ab}$ dependence of T_c determined from the data in (a) by three criteria $10\%\rho_n$, $50\%\rho_n$ and $90\%\rho_n$. The inset shows a sketch map of the field configuration for the measurements. $B_{||ab}$ is applied perpendicular to the current. (c) $B_{||ab}$ (normalized by $B_{||c}$) dependence of the T_c enhancement by the criterion $50\%\rho_n$ under three fixed $B_{||c} = 0.2 \text{ T}$, 0.4 T and 0.8 T .

Table 1: Summary of the upper critical fields (B_{c2}^{ab} and B_{c2}^c) and the paramagnetic limiting field (B_P) of the sample #1.

T_c	$dB_{c2}^{ab}(T)/dT _{T_c}$	$dB_{c2}^c(T)/dT _{T_c}$	B_{c2}^{ab}	B_{c2}^c	B_P
3.17 K	-4.34 T/K	-0.39 T/K	9.5 T	0.86 T	5.8 T

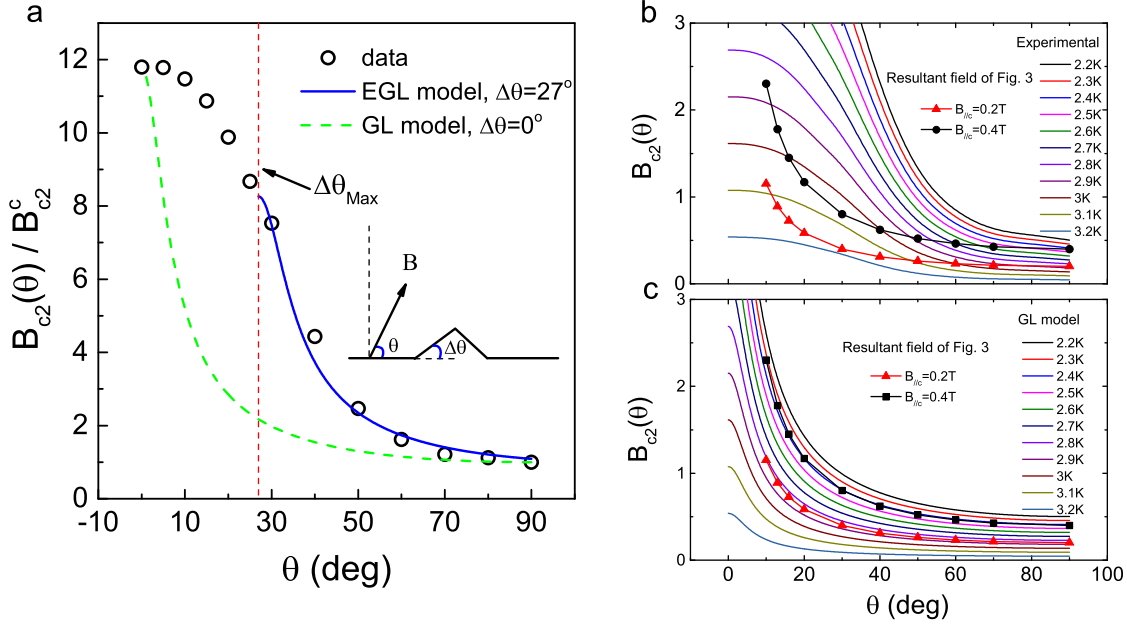


Figure 4: (a) The comparison between the angle dependence of upper critical field and the extended GL (EGL) model considering the influence of the wrinkles. (b) The comparison between the angle dependence of experimental upper critical field and the practical field applied in the experiments shown in Fig. 3. (c) The comparison between the GL model and the practical field applied in the experiments shown in Fig. 3.